Heat Transfer Rates for Filmwise, Dropwise, and Superhydrophobic Condensation on Silicon Substrates

by

Travis M. Hery

SUBMITTED TO THE DEPARTMENT OF MECHANICAL ENGINEERING IN PARTIAL FULFILLMENT OF THE REQUIREMENTS FOR THE DEGREE OF

BACHELOR OF SCIENCE IN MECHANICAL ENGINEERING
AT THE
MASSACHUSETTS INSTITUTE OF TECHNOLOGY

JUNE 2011

Signature of Author: _____
Department of Mechanical Engineering
May 6, 2011

Certified by: _____
Evelyn N. Wang
Assistant Professor
Thesis Supervisor

Accepted by: _____
John H. Lienhard V
Samuel C. Collins Professor of Mechanical Engineering
Undergraduate Officer

Heat Transfer Rates for Filmwise, Dropwise, and Superhydrophobic Condensation on Silicon Substrates

by

Travis M. Hery

Submitted to the Department of Mechanical Engineering
on June 6, 2011 in Partial Fulfillment of the
Requirements for the Degree of Bachelor of Science in
Mechanical Engineering

ABSRACT

Condensation, a two-phase heat transfer processes, is commonly utilized in industrial systems. Condensation heat transfer can be optimized by using surfaces in which dropwise condensation (DWC) occurs, and even further optimized using superhydrophobic surfaces. For superhydrophobic condensation, a structured silicon surface with pillars 2.1 μm tall, 200 nm in diameter, and a 400 nm pitch was tested. By removing noncondensable gases (NCG) from the system by means of a steam trap, the heat transfer rates of DWC and SHC were found to be greater than that of filmwise condensation (FWC) by a factor of 2, but indistinguishable from each other. The effect of NCG leads to a 5x reduction in heat transfer rates for both DWC and SHC. DWC heat transfer rates are as much as 50 kW/m^2 less than FWC at the same temperature difference, representing a 25% reduction. However, the SHC heat transfer rates remain above those of FWC by as much as 50 kW/m^2 at the same temperature difference, representing a 20% improvement. These studies suggest that SHC may be a useful passive method to improve condensation heat transfer rates in the presence of NCG. However, it remains to be seen if SHC can provide better heat transfer rates than DWC under saturated steam conditions.

Thesis Supervisor: Evelyn N. Wang
Title: Professor of Mechanical Engineering

Acknowledgements

I would like to thank my thesis advisor, Professor Wang, for providing me with this opportunity and the support shown throughout the duration of the semester. I would also like to thank Dr. Ryan Enright for providing me with the necessary equipment for my experiments and for providing his expertise to allow me to accomplish my goals. Thanks to Hank Chu for the contact angle measurement for the hydrophilic silicon sample. Thanks to Ahmed Al-Obeidi for fabricating the structured silicon sample.

Table of Contents

Introduction

Condensation is an important heat and mass transfer process that relies on the latent heat of vaporization, resulting in the heat transfer coefficients significantly larger in comparison to sensible heat transfer systems. This phenomenon is used in a number of systems, including heat pipes, power plants, and thermal water desalination. Increased heat transfer rates allow for systems such as these to decrease in size without sacrificing performance, or remain the same size while increasing the performance. Currently, filmwise condensation (FCW), where the new phase condenses as a film covering the heat transfer surface, is most prevalent in industry. However, it is well known that dropwise condensation (DWC), where the new phase nucleates as discrete droplets on the heat transfer surface, can achieve heat transfer rates that are an order of magnitude better than FWC [1].

In order to further increase DWC heat transfer rates, it is desired for as much of the surface to be available for nucleation as possible. Furthermore, it has been experimentally determined that the majority of heat transfer occurs for water droplets smaller than 100 μm in diameter due to the significant thermal resistance of the condensate [2]. Under stagnant or near stagnant vapor conditions, the characteristic droplet shedding size is determined by a balance of gravitational and surface forces. The dimensionless number used to characterize this force balance is the known as the Bond number,

$$Bo = \frac{\Delta\rho g d_w^2}{\gamma}, \tag{1}$$

where $\Delta\rho$, g, d_w, and γ are the difference in density of the saturated liquid and vapor, the gravity constant, diameter of the water droplet, and surface tension, respectively. For DWC where the droplet drips off the surface due to gravity, Bo ≈ 1, Eq. (1) suggests a characteristic shedding diameter on the order of $d_w \approx 1$ mm.

Superhydrophobic surfaces (SHC) are promising candidates for further improving condensation heat and mass transfer rates as they display very large apparent contact angles and low contact angle hysteresis through the combination of hydrophobic surface chemistry and micro- or nanoscale roughness. Recently, it has been found that dropwise condensation

can be achieved on properly designed, nanostructured, superhydrophobic surfaces. A particular feature of superhydrophobic condensation (SHC) is a passive surface-tension-driven mechanism that can reduce the characteristic droplet shedding diameter to $d_w = 10$ μm ($\mathrm{Bo} \approx 1\mathrm{x}10^{-5}$) [3]. This behavior arises due to the fact that as a nucleated droplet on a superhydrophobic surface grows, it will eventually merge with a neighboring droplet. The resulting larger droplet has a reduced curvature. The net decrease in curvature results in a small amount of energy release. Since the droplet is weakly pinned to the surface, a significant portion of the released energy is converted into kinetic energy, resulting in the droplet "jumping" free from the surface. Ejection velocities on the order of 1 m/s have been observed.

In order to determine the likelihood of such jumping behavior on structured surfaces, the energy ratio, E^*, associated with two distinct wetting state can be defined as,

$$E^* = \frac{\cos\theta^{CB}}{\cos\theta^{w}}, \tag{2}$$

where θ^{CB} is the Cassie-Baxter contact angle, associated with weak droplet pinning, and θ^{w} is the Wenzel contact angle, associated with highly-pinned droplets penetrating the surface roughness [4]. The Cassie-Baxter contact angle can be calculated from

$$\cos\theta^{CB} = \varphi^{s}(\cos\theta_e + 1) - 1, \tag{3}$$

where φ^{s} is the pillar solid fraction in contact with a droplet in the weakly pinned wetting state. For a pillar-structured surface, the solid fraction is given by

$$\varphi^{s} = \frac{\pi d^2}{4l^2}, \tag{4}$$

where d is the pillar diameter and l is the pillar pitch (center-to-center) spacing. The equilibrium contact angle, θ_e, is the intrinsic contact angle of the surface at the molecular level.

The Wenzel contact angle is determined from

$$\cos\theta^{w} = r\cos\theta_e, \tag{5}$$

where r is the roughness factor defined as the ratio of the total surface area to the projected area. For a pillar array, the form of this ratio is

$$r = 1 + \frac{\pi dh}{l^2}, \tag{6}$$

where h is the height of the pillars. If $E^* < 1$, it is more probable that the droplets will weakly pin to the surface. If $E^* > 1$, it is more probable that the droplets will penetrate the pillars and remain pinned to the surface during droplet merging.

In order to investigate the efficacy of such a droplet shedding mechanism on the condensation heat transfer process, rates for FWC, DWC, and SHC were measured using a copper bar calorimeter apparatus for two distinct noncondensable gas (NCG) levels. In the next section, theory is presented for FWC heat transfer and the upper bound for heat transfer based on the kinetic limit for interphase mass transfer.

Theoretical Analysis

Film Condensation

For FWC on a vertical surface, a layer of liquid builds up on the surface. The thickness of this layer increases the further down the length of the surface, as a result of gravity pulling the liquid above it down and liquid continuing to condense on top of this already condensed liquid. The thickness of this liquid film can be determined as a function of the length down the surface by

$$\delta = \left[\frac{4k_l\mu_l x(T_{sat}-T_w)}{\rho_l(\rho_l-\rho_v)gh_{lv}}\right]^{1/4}, \tag{7}$$

where k_l, μ_l, x, T_{sat}, T_w, ρ_l, ρ_v, g, and h_{lv} are the liquid thermal conductivity, liquid viscosity, distance down the surface from the top, saturation temperature, wall or surface temperature, liquid density, vapor density, gravitational constant, and latent heat of vaporization, respectively [5].

This layer of liquid requires the heat to travel through it before it is able to reach the surface, resulting in an additional thermal resistance being added to the system. This thermal resistance is constantly increasing down the length of the surface. The local Nusselt number can be calculated as a function of the film thickness and is given by [5]

$$Nu = \left[\frac{\rho_l(\rho_l-\rho_v)gh_{lv}x^3}{4k_l\mu_l(T_{sat}-T_w)}\right]^{1/4}, \tag{8}$$

where

$$Nu = \frac{hl}{k} = \frac{q''x}{k\Delta T}, \tag{9}$$

h is the heat transfer coefficient, q'' is the heat transfer rate per unit area, and $\Delta T = T_{sat} - T_s$ is the difference between the saturation temperature and the surface temperature. The heat transfer coefficient scales inversely with the distance down the surface. Therefore, it is desirable to have a surface that is very long horizontally and short vertically to increase the heat

transfer as much as possible. The local Nusselt number can be integrated over the vertical length of the surface to determine the average Nusselt number given by [5]

$$\overline{Nu} = 0.943 \left[\frac{\rho_l(\rho_l-\rho_v)gh_{lv}x^3}{k_l\mu_l(T_{sat}-T_w)}\right]^{1/4}. \quad (10)$$

Interfacial Limit

During drop-wise condensation on an inclined plate, liquid nucleates and grows to form a spherical cap geometry, defined by the contact angle. The formation of droplets as opposed to a film leaves a portion of the surface open for the vapor to condense onto. The heat does not have to travel through the liquid at all points on the surface and the thermal resistance of drop-wise condensation can be significantly less than that of film condensation.

Conceptually, as the average droplet size on the surface becomes smaller, more of the surface is exposed for nucleation to occur, and the heat transfer rates in a saturated environment will approach a maximum. Disregarding resistances associated with surface coatings and heat flux non-uniformity, this maximum heat transfer rate is ultimately limited by the rate at which water molecules can be added at the interface to the condensed phase. This maximum heat transfer rate is given by

$$q'' = \left(\frac{2\hat{\sigma}}{2-\hat{\sigma}}\right)\left(\frac{h_{lv}^2}{T_{sat}v_{lv}}\right)\left(\frac{M}{2\pi\bar{R}T_{sat}}\right)^{1/2}\left(1-\left(\frac{P_v v_{lv}}{2h_{lv}}\right)\right)(T_{sat}-T_w), \quad (11)$$

where $\hat{\sigma}$ is the condensation sticking coefficient (equivalent to 1 in the ideal case of pure interfaces), v_{lv}, M, $\bar{R}$, and P_v are the difference in specific volumes between vapor and liquid form, molecular weight, universal gas constant, and vapor pressure, respectively [5]. This thermal resistance is much smaller than the resistances associated with heat conduction through water on the surface and the effects of noncondensable gases, described below, and it is ignored in most cases. However, it may be possible to approach this limit through the proper design of SHC surfaces.

Noncondensable gases

When a vapor condenses onto a surface, there is a significant drop in volume that the fluid particles occupy. With this drop in volume, there is a coinciding drop in pressure. This drop

in pressure causes noncondensable gases (NCG) to move toward the condensing surface to maintain the total equilibrium pressure. NCG do not condense under typical water condensation conditions and remains next to the surface at a higher concentration than the bulk as long as the vapor is condensing. The presence of the NCG leads to a mass diffusion resistance for water vapor moving from the bulk to the condensing surface, greatly reducing mass and, thus, heat transfer rates since $q'' = \dot{m}h_{lv}$, where $\dot{m}$ is the mass flow rate of water to the condensing surface [5].

Ideally, the best way to avoid the effects of NCG is by entirely removing them from the condensation environment. However, this may not always be possible and a number of approaches can be taken in order to reduce or avoid the effects of the NCG. A turbulent flow can be introduced into the condensing vapor, effectively washing away the non-condensable gases from the surface. Nominally, any method that induces boundary layer mixing to break up the diffusive field should improve condensation rates [6].

Experimental Procedure

Sample Manufacturing and Preparation

Smooth samples measuring 2x2 cm were cut from a polished silicon wafer with a nominal thickness of 650 μm. The samples were then rinsed with acetone, isopropyl alcohol, methanol, ethanol, and deionized water. Next, the samples were dried using pure nitrogen gas and placed in a plasma cleaner (Harrick Plasma, PDC-002) for 30 min to remove any remaining organics on the surface. The cleaned silicon samples had a measured equilibrium contact angle of $\theta_e = 39.5 \pm 1.5°$. Some of the smooth samples were then functionalized with a self assembling monolayer (SAM) of (Tridecafluoro-1,1,2,2-Tetrahydrooctyl)-1-Trichlorosilane supplied by United Chemical Technologies. The samples were functionalized by placing them in a vacuum chamber with the liquid silane for 25 minutes to allow for condensation of the silane molecules on to the sample surface. These molecules form a covalent bond via silanol groups (Si-OH) at the surface. For the silane functionalized silicon surfaces, an equilibrium contact angle of $\theta_e = 103° \pm 2.3°$ was measured.

A pillar-structured silicon sample was fabricated using interference lithography and interfacial wet etching. A photoresist mask was designed on the surface using interference fringes on a Lloyd's mirror setup, in which the photo-resist was exposed to fringe patterns orientated at 90° to one another to define a dot array. The surface was then coated with a layer of gold, approximately 100 nm thick. A lift-off process using acetone was then performed to remove the photoresist-defined dot array. This leaves an anti-dot array in the gold film where the silicon pillars were eventually created. The sample was then placed in a hydrofluoric acid bath. While in the bath, chemical wet-etching occurred between the gold and silicon interface, leaving behind silicon pillars at the anti-dot locations. The resulting pillar geometry can be seen in Fig. 1 below.

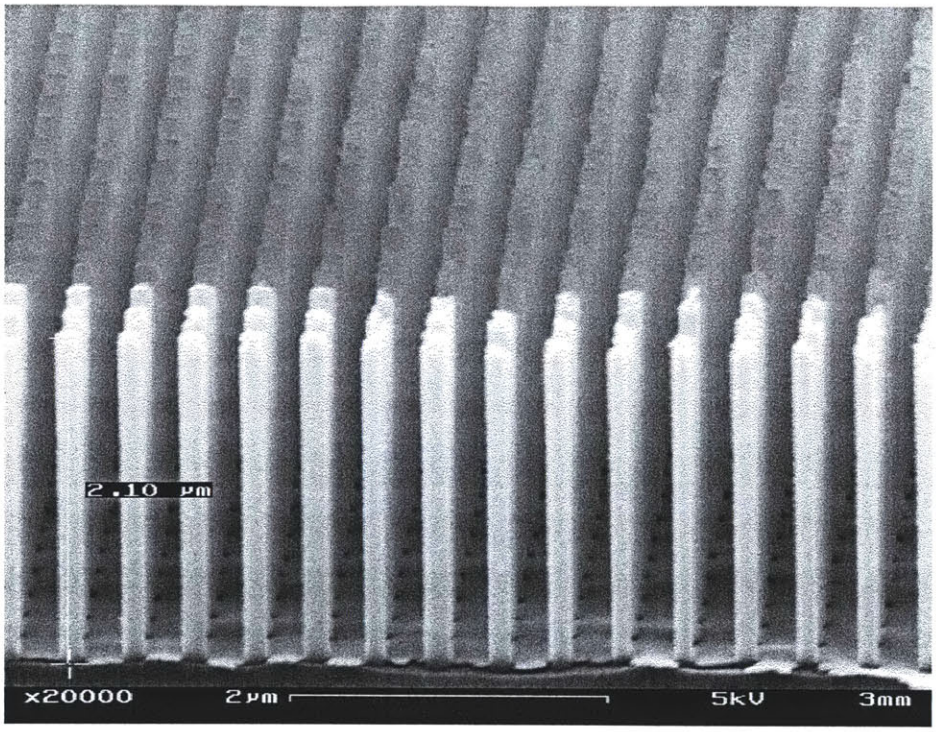

Figure 1: Silicon pillars formed after the interfacial etching process with dimensions of l = 400 nm, d = 200 nm, and h = 2.1 µm. The gold film is visible at the base of the pillars.

The height of the pillars was determined by the etching time in the hydrofluoric acid bath, and the diameter and pitch were determined by the interference pattern used in the beginning of the process. For this sample, the height of the pillars was 2.1 µm, the diameter of the pillars was 200 nm, and the pitch was 400 nm.

The structured silicon was then functionalized with silane as described above. After the silane application, the surface was placed in a 1mM solution of thiol (1H,1H,2H,2H-Perfluorodecanethiol, Sigma-Aldrich) in pure ethanol and left to sit of 45 minutes to form a hydrophobic SAM on the gold film. The surfaces were then taken out and rinsed off with ethanol and deionized water and dried with pure nitrogen gas. Considering the final dimensions of the pillar array and the wettability of the functional SAM's, Eq. (2) predicts $E^* = 0.41$, suggesting that the surface should be stable for SHC. Next, the experimental set-up and procedure for measuring condensation heat transfer rates is detailed.

Apparatus and Data Collection

Heat flux and surface temperature measurements were made using the copper bar shown in Fig. 2. The bar was 95 mm long. For the first 75 mm on the front side, the side the sample was attached, the bar had a width and height of 20 mm. The next 15 mm the bar had a fillet to expand in width and height. For the last 5 mm, the back side of the copper bar, it had a constant height of 64 mm and width of 102 mm. The outside of the bar was covered with an insulating material to prevent heat loss along the length of the bar, leaving the front and back surfaces exposed. A total of 16 type T thermocouples with a calibrated uncertainty of ±0.2 °C were used at specific lengths along the bar at a depth of 10 mm, allowing for accurate temperature readings at known distances in the copper.

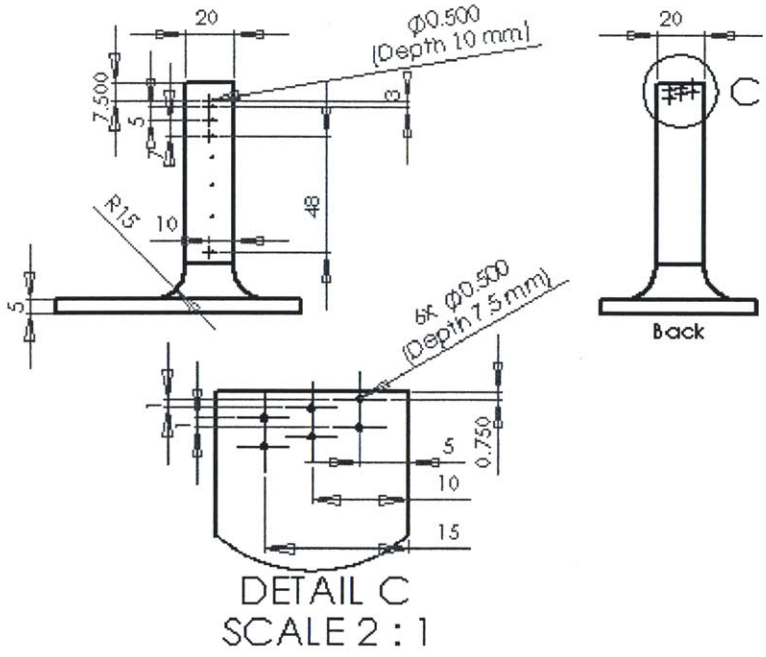

Figure 2: Drawing of the copper bar used for measuring q'' and T_s, Units are in millimeters.

The copper bar was wrapped in insulation and integrated into the set-up shown in Fig. 3. Attached to the back side of the copper bar was a liquid heat exchanger (CPU-300-V10, Koolance) with a manufacturer-stated thermal resistance of 0.07±0.005 °C/W.

Water was circulated via insulated tubing through the liquid heat exchanger at a temperature set by a recirculating temperature control bath (Ecoline 310, Lauda). The water bath temperature was set to between 80 and 90 °C at the beginning of each experiment and then lowered at a rate of between 0.5 and 0.167 °C/min, until it reached a temperature of between 0 and 10 °C.

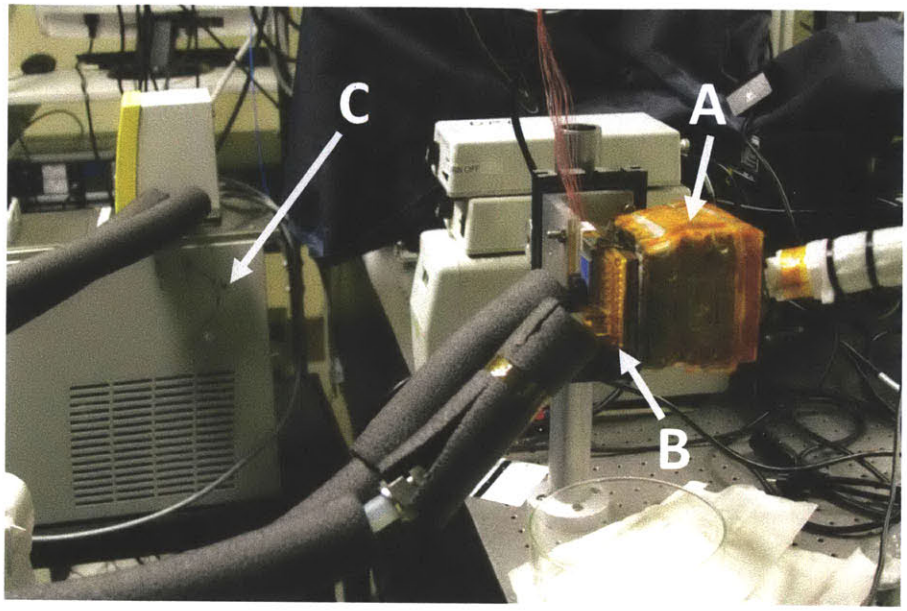

Figure 3: Back side of the condensation apparatus with the insulated copper calorimetry bar (A), the liquid heat exchanger (B), and the temperature control bath (C).

The sample to be tested was attached to the front side of the copper bar. In order to reduce contact resistance and securely attach the sample to the copper bar, thermal grease was used. The thermal grease was placed on the front surface of the copper and smoothed to give a thickness of 50 ± 25 μm. The sample was then attached in such a way to prevent the formation of air pockets between the sample and the thermal grease. Any excess grease was then removed to prevent contamination of the sample surface.

Steam for the condensation process was created from water in an insulated filtering flask sitting on a hotplate (Thermo Scientific, Cimarec) set to 500 °C. The top of the flask was closed off by a rubber stopper, leaving the side, glass tube opening as the only exit for the produced steam. A tube was attached to the end of the opening on the flask. Upon reaching

boiling conditions in the flask, the steam flowed through the length of the tube towards the sample. The tube was covered with insulation to reduce heat loss and lined with electric guard heaters to prevent premature condensation of the steam while still in the tube. The opposite end of the tube was aimed at the sample on the front of the copper bar, allowing for full contact of the sample with the steam, as seen in Fig. 4 below.

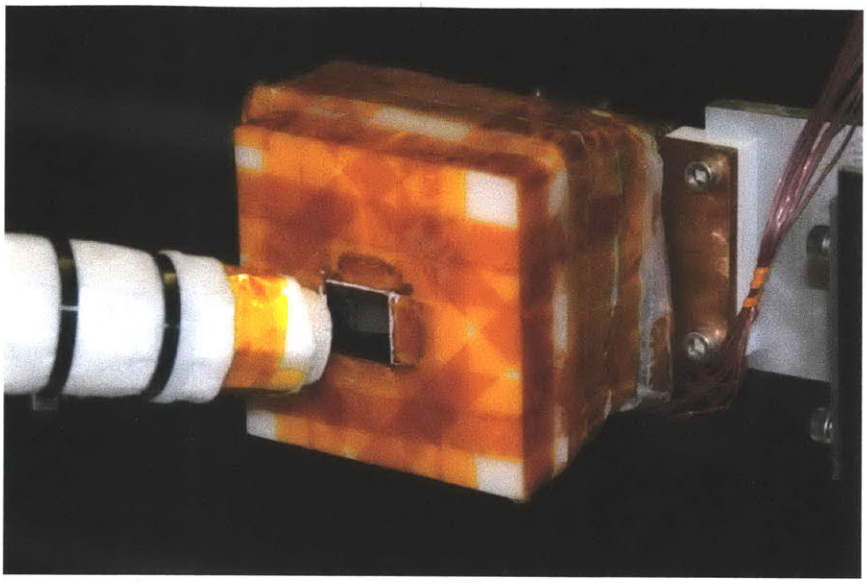

Figure 4: End of steam tube aimed at sample surface, allowing for condensation to take place.

With the saturated steam condensing on the sample surface on the front side of the copper and the liquid heat exchanger on the back side of the copper, a temperature gradient was created along the length of the copper. This temperature gradient was determined from the temperatures recorded at the thermocouples and the known positions of these thermocouples. With the known thermal conductivity of copper (k_{Cu} = 396 W/m-K), the heat flux was calculated from Fourier's conduction law,

$$q'' = k_{Cu}\frac{dT}{dx}. \tag{12}$$

Using the heat flux, thicknesses, and thermal conductivities of the copper, thermal grease, and sample, and Eq. 12, the difference in temperature between the surface, T_s, and the closest thermocouple, T_1, to the surface of the sample was calculated

$$T_s - T_1 = \sum_{i=1}^{3} \frac{\Delta x_i q''}{k_i}. \quad (13)$$

This allowed for the analysis of heat flux compared to the difference in temperatures of the saturated steam and sample surface. There were errors associated with the heat flux and the surfaces temperature measurements were determined using the Kline-McClintock method [7].

The first thermal grease used was Omegatherm 201 from Omega Engineering, which had a manufacturer-stated thermal conductivity of k_{g1} = 2.3 W/m-K, which resulted in temperature gradients within the grease alone of up to 10 °C. This resulted in larger uncertainties when calculating the surface temperature of the sample. It was also a limiting factor in the maximum heat flux achievable by the experimental set-up due to the finite temperature difference between the steam and the recirculating bath. In order to mitigate these issues, a second thermal grease, Cool Silver from AI Technology, was used in later experiments, which had a manufacturer-stated thermal conductivity of k_{g2} = 12 W/m-K, almost six times as much as the first thermal grease. This greatly reduced the uncertainty in calculating the surface temperatures and allowed for higher heat fluxes to be achieved.

After running several tests on a number of different samples, it became apparent that the apparatus as described above was not sufficient. The NCG within the atmosphere were able to come into contact with the sample, even with the steam directed at it. To keep the noncondensable gases away from the sample, a simple form of a steam trap was used. An enclosure was placed on the end of the steam tube and around the sample. This allowed for steam to leave the enclosure, but prevent the air from entering, ensuring that only steam came into contact with the sample. The enclosure was covered with two heating pads and insulation to prevent condensation along its walls. An additional thermocouple, covered in an absorbent material, was placed next to the sample surface to record the wet bulb temperature T_{wb} within the steam trap. It was found that the typical wet bulb temperature increased from ~90 °C to 100 °C with the incorporation of the steam trap. The final configuration of the experimental apparatus can be seen in Fig. 5 below. The steam tube was attached to the steam trap on the left, which extended to the filtering flask. The sample was enclosed by the right of the steam trap, attached to the insulation wrapped, copper bar.

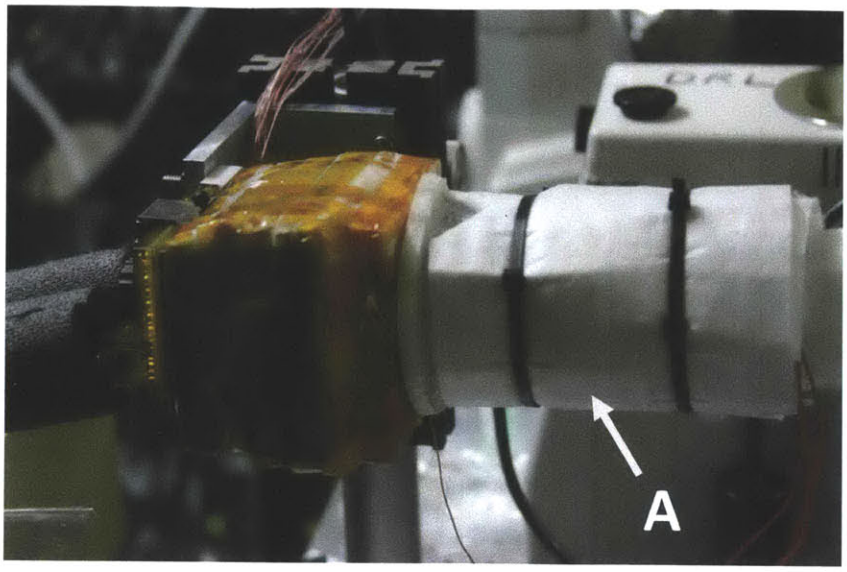

Figure 5: Final configuration of the condensation apparatus, with controlled temperature water flow on the back, and a steam trap (A), with a constant supply of steam on the front.

Results and Discussion

The heat transfer rates FWC were obtained with both thermal greases in the presence of NCG to determine the discrepancies between the two. The results are shown in Fig. 6 below.

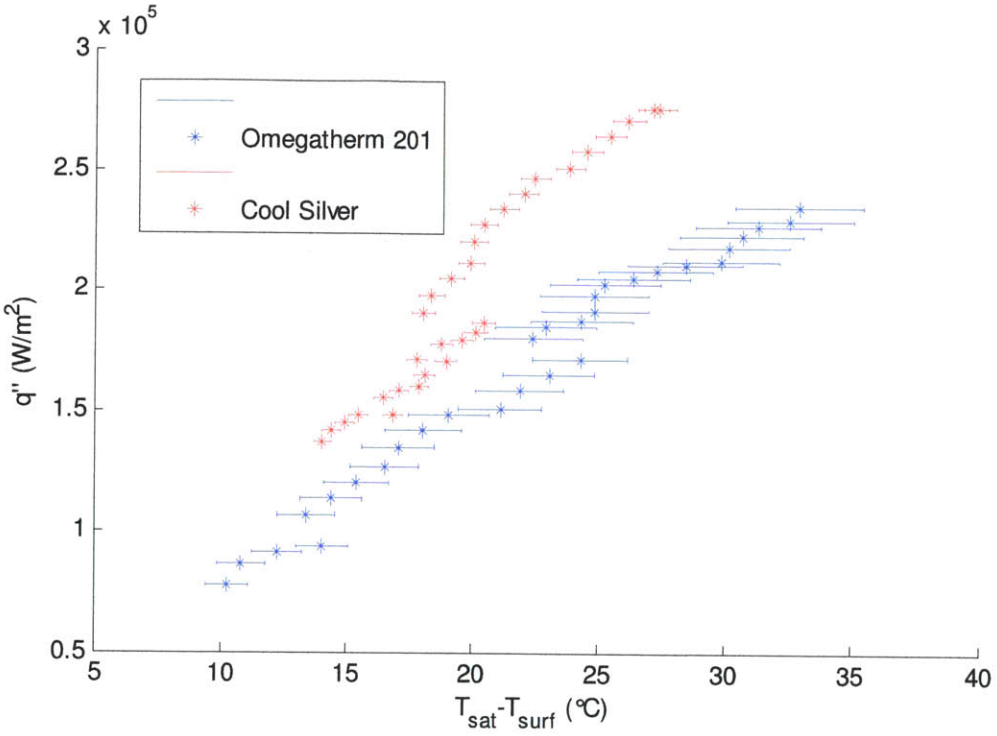

Figure 6: Comparison of heat transfer rates in the presence of noncondensable gases on cleaned silicon sample using different thermal greases.

The maximum heat flux using the new grease was higher than when using the old grease. Also, the new grease resulted in a lower uncertainty for the surface temperature. This was due to the higher thermal conductivity, resulting in lower temperature gradients across the grease.

For testing without the presences of NCG, the samples were attached to the copper using the Cool Silver thermal grease and were placed under the steam trap. The heat transfer rates for varying surface temperatures of the three samples were recorded. These heat transfer rates were compared to Nusselt film theory heat transfer and the maximum interfacial heat transfer in Fig. 7 below.

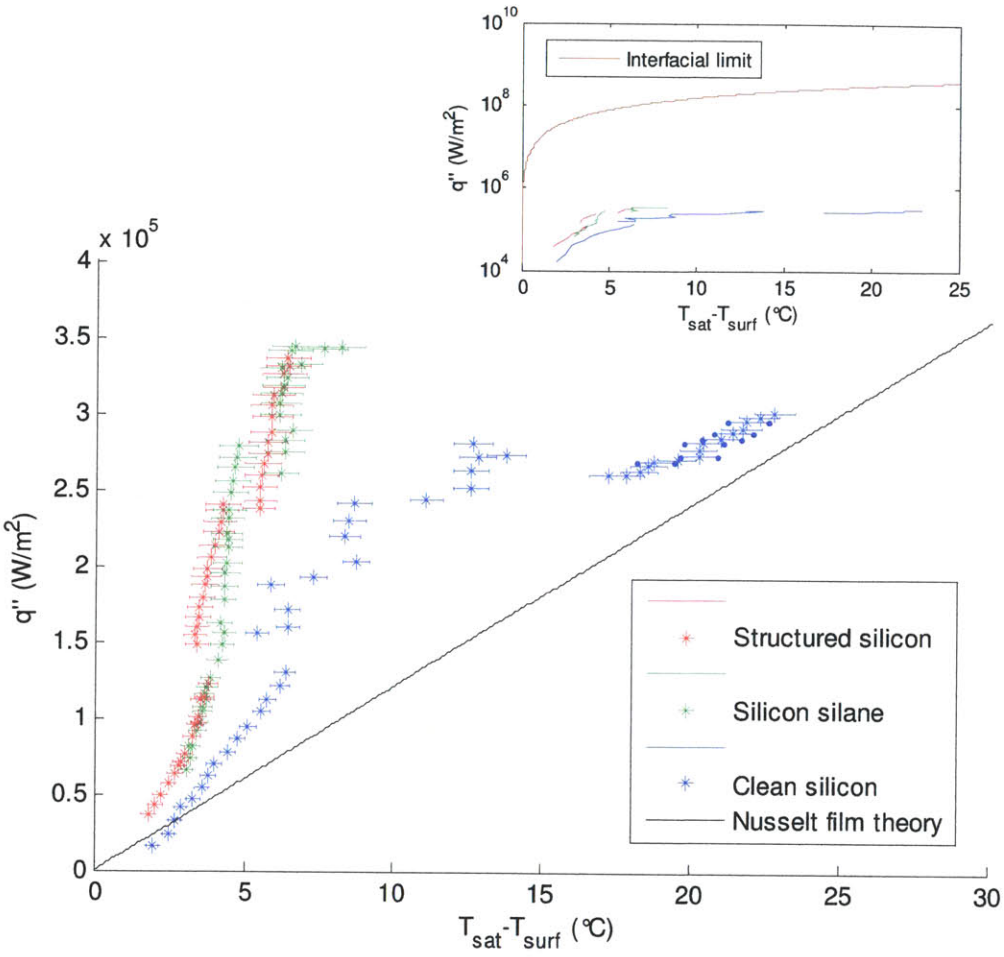

Figure 7: Heat flux for the three different samples without the presence of NCG, as well as the heat flux predicted by Nusselt film theory and the interfacial heat transfer limit (inset).

From the results, the film condensation of the clean silicon sample had transfer rates which were comparable to the Nusselt film theory, which was expected. However, the data was very spread out in some areas. This may be a result of the temperature ramp rate of the temperature bath being too large. A lower ramp rate would be expected to give much clearer data. The heat transfer rates for DWC and SHC were greater than that of FWC, by a factor of about 2. There was no significant difference in the heat transfer rates for DWC and SHC, and the heat transfer rates of these two samples still fall short of the interfacial heat transfer limit. It should be noted that the DWC and SHC results are in the middle range of previously measured heat transfer rates [2] suggesting that a small, but significant, amount of NCG was

still present in the system that could not be resolved by the wet bulb temperature measurement.

The heat transfer rates of the three samples were also obtained in the presence of NCG, without the steam trap, with a measured T_{wb} = 86 °C – 96 °C. The samples were attached to the copper using the Omegatherm 201 thermal grease. These results are shown in Fig. 8.

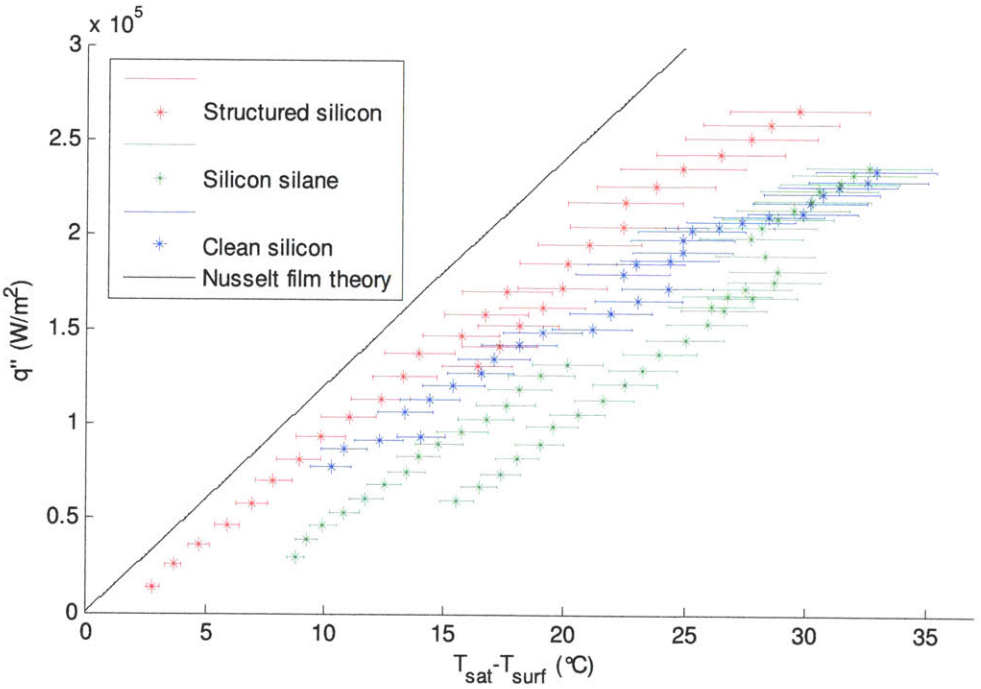

Figure 8: Comparison of the heat transfer behavior of the three samples and Nusselt film theory in the presence of noncondensable gases.

In the presence of NCG, the heat transfer rates of all the samples were lower than without NCG and the prediction of Nusselt film theory, which, in the form used here, does not consider the presence of NCG. The heat transfer rates for the DWC and SHC dropped by more than a factor of 5 when in the presence of NCG. The DWC heat transfer rates were at most 50 kW/m^2 below that of FWC for the same temperature difference, a 25% reduction. This demonstrates that the thermal resistance associated with the presence of NCG for DWC overcomes the advantage typically seen with this type of condensation. However, the heat transfer rates of the SHC started off similar to the clean silicon and got up to 50 kW/m^2 greater at a temperature difference of 30 °C, a 20% improvement. Two possible explanations for this result are an

improvement simply due to the increase in available area since $r \approx 8$ or may be associated with the jumping droplet phenomena inducing mixing in the NCG boundary layer.

Conclusions

It is possible to minimize the NCG from the area of condensation by the use of a steam trap. Without the presence of NCG, the heat transfer rates of DWC and SHC increase by more than a factor of 5. The FWC heat transfer rates will not see such an increase, due to the weak effect of NCG on FWC. In this type of environment, both DWC and SHC will be greater FWC.

Typically, higher heat transfer rates can be attained with DWC than can be attained with FWC. However, due to the presence of NCG, the heat transfer rates for DWC can drop below that of FWC. However, SHC was shown to maintain heat transfer rates larger than that of FWC in the presence of NCG.

It remains to be seen if SHC can provide larger heat transfer rates than DWC when NCG are minimized. It is presumed that the heat transfer rates of SHC can surpass those of DWC at high heat fluxes and an optimized surface design.

Recommendations

Even with the use of a steam trap and wet bulb temperature measurement, accurate quantification of the amount of NCG at the sample surface was not possible. In order to entirely eleminate NCG, the condensation experiments should be run in a controlled environment that is completely shut out from the surrounding atmosphere. The percentage of NCG in the environment can then be controlled and accurately measured. A detailed analysis of the effect of NCG levels on the surface can be obtained.

The temperature ramp during experimentation should be as small as possible. The slower the change in temperature, the more accurate the data became and less noise was introduced into the measurements. As such, a larger filtering flask should be used for the purpose of having a larger reservoir of water. Having a larger amount of water to boil will allow for longer run times of the experiment. Longer run times will provide more consistent data by allowing the ramp rate to be reduced.

Bibliography

1) B. Chung, M. C. Kim, and M. Ahmadinejad. "Filmwise and dropwise condensation of steam on short inclined plates." *Journal of Mechanical Science and Technology.* **Vol. 22.** (2008).

2) W. M. Rohsenow, J. P. Hartnett, and E. N. Ganić. "Handbook of heat transfer fundamentals." McGraw-Hill, Inc. 1985.

3) J. B. Boreyko and C. Chen. "Self-Propelled Dropwise Condensate on Superhydrophobic Surfaces." *Physical Review Letters.* **Vol. 103**. No. 184501. (2009).

4) D. Quere. "Wetting and Roughness." *Annual Review of Materials Research.* **Vol. 38.** (2008)

5) V. P. Carey. "Liquid-Vapor Phase-Change Phenomena: An Introduction To The Thermophysics Of Vaporization and Condensation Processes in Heat Transfer Equipment." Taylor & Francis, Inc., 2007.

6) X. Ma, X. Zhou, Z. Lan, Y. LI, Y. Zhang. "Condensation heat transfer enhancement in the presence of non-condensable gas using the interfacial effect of dropwise condensation." *International Journal of Heat and Mass Transfer.* **Vol. 51**. (2008).

7) Kline, S. J., and F. A. McClintock. "Describing Uncertainties in Single-Sample Experiments." *Mechanical Engineering.* **Vol. 75**. No. 1. (1953).